TU Delft

Delft University of Technology

Lanthanopolyoxometalate-Silica Core/Shell Nanoparticles as Potential MRI Contrast Agents

Carvalho, Rui F.S.; Pereira, Giovannia A.L.; Rocha, João; Castro, M. Margarida C.A.; Granadeiro, Carlos M.; Nogueira, Helena I.S.; Peters, Joop A.; Geraldes, Carlos F.G.C.

DOI
10.1002/ejic.202100445

Publication date
2021

Document Version
Accepted author manuscript

Published in
European Journal of Inorganic Chemistry

Citation (APA)
Carvalho, R. F. S., Pereira, G. A. L., Rocha, J., Castro, M. M. C. A., Granadeiro, C. M., Nogueira, H. I. S., Peters, J. A., & Geraldes, C. F. G. C. (2021). Lanthanopolyoxometalate-Silica Core/Shell Nanoparticles as Potential MRI Contrast Agents. *European Journal of Inorganic Chemistry*, *2021*(34), 3458-3465. https://doi.org/10.1002/ejic.202100445

Important note
To cite this publication, please use the final published version (if applicable).
Please check the document version above.

Copyright
Other than for strictly personal use, it is not permitted to download, forward or distribute the text or part of it, without the consent of the author(s) and/or copyright holder(s), unless the work is under an open content license such as Creative Commons.

Takedown policy
Please contact us and provide details if you believe this document breaches copyrights.
We will remove access to the work immediately and investigate your claim.

This work is downloaded from Delft University of Technology.
For technical reasons the number of authors shown on this cover page is limited to a maximum of 10.

Lanthanopolyoxometalates-silica core/shell nanoparticles as potential MRI contrast agents

Rui F. S. Carvalho,[a] Giovannia A. L. Pereira,[a,b,&] João Rocha,[b] M. Margarida C. A. Castro[a,c] Carlos M. Granadeiro,[b,%] Helena I.S. Nogueira,[b] Joop A. Peters,[d] and Carlos F. G . C. Geraldes*[a,c,e]

[a] Rui F. S. Carvalho, Dr. Giovannia A. L. Pereira, Prof. Dr. M. Margarida C. A. Castro, Prof. Dr. Carlos F. G. C. Geraldes
Department of Life Sciences, Faculty of Science and Technology, University of Coimbra, Calçada Martim de Freitas, 3000-393 Coimbra, Portugal
E-mail: ruifscarvalho@gmail.com, giovanniapereira@ufpe.br, gcastro@uc.pt, geraldes@ci.uc.pt

[b] Dr. Giovannia A. L. Pereira, Prof. Dr. João Rocha, Dr. Carlos M. Granadeiro, Prof. Dr. Helena I.S. Nogueira
CICECO, Aveiro Institute of Materials, Department of Chemistry, University of Aveiro, 3810-193 Aveiro, Portugal
Email: rocha@ua.pt, cgranadeiro@fc.up.pt, helenanogueira@ua.pt

[c] Prof. Dr. M. Margarida C. A. Castro, Prof. Dr. Carlos F. G. C. Geraldes
Coimbra Chemistry Center, Rua Larga, University of Coimbra, 3004-535 Coimbra, Portugal

[d] Dr. Joop A. Peters
Department of Biotechnology, Delft University of Technology, Van der Maasweg 9, 2629 HZ Delft, The Netherlands

[e] Prof. Dr. Carlos F. G. C. Geraldes
CIBIT/ICNAS - Instituto de Ciências Nucleares Aplicadas à Saúde, Pólo das Ciências da Saúde, Azinhaga de Santa Comba, 3000-548 Coimbra, Portugal

***** Corresponding author: geraldes@ci.uc.pt

[&] Present address: Fundamental Chemistry Department, UFPE, Recife, Pernambuco, Brazil

[%] Present address: LAQV-REQUIMTE, Department of Chemistry and Biochemistry, Faculty of Sciences, University of Porto, Rua do Campo Alegre, 4169-007 Porto, Portugal

Abstract

The NMR relaxivities of the decatungstolanthanoates core-shell nanoparticles, prepared by encapsulating $[Ln(W_5O_{18})_2]^{9-}$ polyoxometalates (LnPOM) within amorphous silica shells ($K_9[Ln(W_5O_{18})_2]@SiO_2$), were studied along the Ln series. The relaxivity of GdPOM is slightly higher than for Gd-DTPA due to second-sphere relaxation effects, but the values for the other paramagnetic LnPOMs are much smaller due to the short T_{1e} values of their Ln^{3+}-ions. The NPs have core-shell spherical structures, with LnPOM-containing cores with 9.5 - 28 nm diameters, and 4.0-11.0 nm thick amorphous silica shells. In water suspensions, the NPs have negative zeta potentials (-32.5 to -40.0 mV) and time-dependent hydrodynamic diameters (31-195 nm) reflecting the formation of aggregates. The relaxivities of $GdPOM@SiO_2$ NPs suspensions (r_1 = 10.97 $(mM\ Gd)^{-1}\cdot s^{-1}$, r_2 = 12.02 $(mM\ Gd)^{-1}\cdot s^{-1}$, 0.47 T, 25 ^oC) are considerably larger than for the GdPOM solutions, indicating that their silica shell is significantly porous to water. This increase is limited by the agglomeration of the complexes in the NPs core, limiting their access to water to those at the core surface. Replacing half of the Gd^{3+} ions by Eu^{3+} decreases the NPs r_1 and r_2 relaxivities at 0.47 T to 20 % and 35 % of their initial values, which are still considerable, but does not affect the efficient luminescence properties of the Eu^{3+} centres. This indicates that the mixed NPs have potential as dual modality MRI/optical imaging contrast agents.

Introduction

Molecular imaging applications of Magnetic Resonance Imaging (MRI), although favoured by the high spatial resolution (μm) of the technique, are limited by its low sensitivity.[1] This may preclude the visualization of disease biomarkers, which often depends on receptors that are present on cell surfaces at very low concentrations, typically in the range of 10^{-10}–10^{-7} mol kg^{-1},[2] below the detection limit of contrast agents (CAs) containing a single Gd^{3+}-ion per molecule.[3,4] In order to detect molecular events at the cellular level (in the nanomolar concentration range), a high CA payload must be delivered at the target site. Magnetic nanoparticulate CAs can deliver a high payload of paramagnetic metal ion (M^{n+}) reporters to the target sites provided they reach them. [5] Rather than the usual relaxivity r_i (i=1,2) in s^{-1} mM^{-1} M, their efficacy as MRI CAs is better expressed by r_i in s^{-1} g^{-1} material (relaxivity density)[6] or in relaxivity per nanoparticle (NP) (= $r_i \times$ number of M^{n+} ions per NP). They have a wide range of applications and, depending on r_2/r_1 ratios, they can be useful as CAs for T_2-weighted (negative contrast) and/or T_1-weighted (positive contrast) imaging. [7] Their *in vivo* pharmacokinetics depends on their particle size and targeting capabilities. [8]

Most paramagnetic inorganic nanomaterials that have been studied as potential MRI CAs are based on water-insoluble Gd^{3+} salts, such as Gd_2O_3 [9,10] and $GdPO_4$,[11,12] Gd^{3+} (or Gd^{3+}-chelate) loaded NPs based on gold or other metals,[13-17] silica (microporous or mesoporous),[18-22] hydrophilic organic colloids,[23] zeolites,[24,25] carbon nanotubes,[26] fullerenes,[27] etc. NPs doped with other Ln^{3+} (such as Eu^{3+}, Dy^{3+} or Ho^{3+}) have also been studied, [28] including silica, [29,30] zeolites [31] and metal-organic frameworks (MOFs). [32]

Removal of a MO^{4+} unit from a polyoxometalate (POM) gives an anion, which can act as a water-soluble inorganic ligand for metal ions. For example, lanthanide ions can be sandwiched by two lacunary Lindqvist anions to form heteropolyanionic complexes with molecular formula $[Ln(W_5O_{18})_2]^{9-}$ (Figure 1A).[33] Ln^{3+} ions are chemically very similar and consequently, the $[Ln(W_5O_{18})_2]^{9-}$ species are almost isostructural, with a central Ln^{3+} ion coordinated to four oxygen atoms of each POM ligand, and with no water molecules in the first coordination sphere of the Ln^{3+}.[34,35] Each of these complexes has his own characteristic physico-chemical properties. For example, the La^{3+} and Lu^{3+} complexes are diamagnetic, whereas the other Ln^{3+} complexes are paramagnetic due to the unpaired

f-electrons. Another example is the diversity of the photophysical properties of Ln^{3+} complexes, [36] where generally the optimal luminescence behavior is found for Tb^{3+} and particularly for Eu^{3+}. The $[Eu(W_5O_{18})_2]^{9-}$ complex has the highest quantum yield of all luminescent POMs described. [37] This is attributed to the absence of quenching water molecules in the first coordination sphere of Eu^{3+}, in addition to an efficient energy - transfer process promoted by an intense O→W ligand-to-metal charge transfer resulting in a strong Eu^{3+} emission. [37,38]

The $K_9[Gd(W_5O_{18})_2]$ POM has been evaluated as an MRI CA for *in vitro* and *in vivo* applications. [39] Even if the central Gd^{3+} ion has no water molecules in its first coordination sphere, the r_1 relaxivity of this compound is slightly higher than Gd-DTPA (Magnevist®), one of the most applied clinical MRI contrast agents. Other Gd^{3+}-containing POMs exhibit even higher r_1 relaxivities, [40-41] and are efficiently taken up by the liver *in vivo*. The LD_{50} of $K_9[Gd(W_5O_{18})_2]$ shows that this POM is more toxic than the clinically used MRI Gd^{3+}-based contrast agents (GBCAs). [39] It is known that the thermodynamically more stable phosphorus-containing POMs rapidly decompose in the serum. [42,43] Therefore, it is anticipated that $K_9[Gd(W_5O_{18})_2]$ may leach significant amounts of free Gd^{3+} *in vivo*, and this poses the risk of developing serious nephrogenic systemic fibrosis (NSF). [44] Furthermore, $K_9[Gd(W_5O_{18})_2]$ has a high osmolality, which may lead to discomfort and adverse effects for the patient, upon intravenous administration. [45] These drawbacks can be removed by coating the POM particles with a silica shell (Figure 1B), with the additional benefit that functional groups may be attached to the silica surface, for targeting. The preparation of core-shell nanocomposites, $Na_9[Ln(W_5O_{18})_2]@SiO_2$ (Ln = Eu, Gd, Tb) with a uniform size distribution using a reverse microemulsion method has been described. [46] The Eu^{3+} and Tb^{3+} containing particles exhibit interesting luminescent properties, which are not significantly disturbed by co-doping with Gd^{3+}.

MRI has excellent spatial and temporal resolution and penetration depth but an inherent low sensitivity for CAs. These properties are complementary to other techniques, such as optical imaging, X-ray computer tomography (CT), and nuclear imaging. Mixing two single-modality CAs is usually not an option because the biodistribution of the two agents is usually different. Although almost all combinations

of imaging techniques are under investigation, the most promising are MRI-PET, MRI-SPECT and MRI-optical imaging. [47-49]

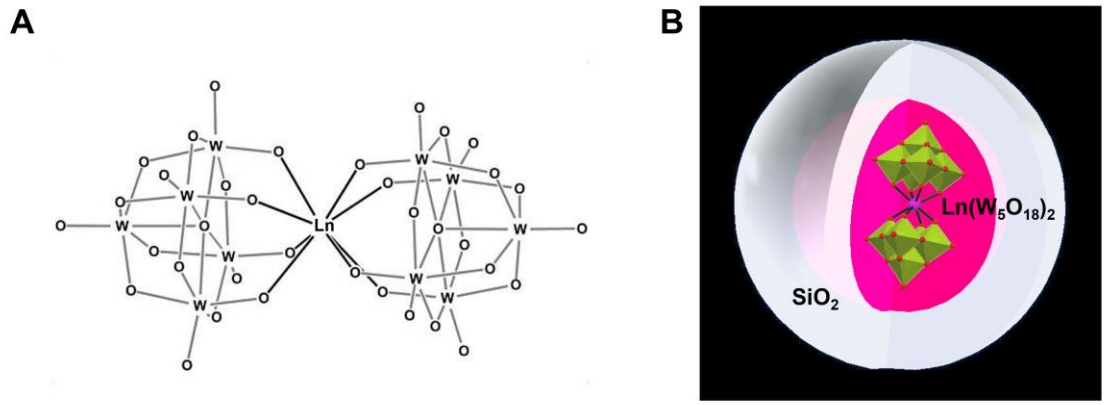

Figure 1. Schematic representation of the A) molecular structure of $[Ln(W_5O_{18})_2]^{9-}$; and B) $Na_9[Ln(W_5O_{18})_2]@SiO_2$ nanocomposite particles.

Here we report on the potential of $Na_9[Ln(W_5O_{18})_2]@SiO_2$ NPs to be used as dual modality CAs in MRI and optical imaging. The characterization of the $Na_9[Ln(W_5O_{18})_2]@SiO_2$ NPs along the lanthanide series in the solid state and in aqueous suspensions complements a previous characterization of the systems with Ln = Eu, Gd and Tb.[46] This is followed by a preliminary evaluation of their longitudinal and transverse relaxation properties for the different lanthanides, and their comparison with the corresponding $Na_9[Ln(W_5O_{18})_2]$ POM aqueous solutions.

Results and Discussion

Characterization of the LnPOMs and LnPOM@SiO_2 nanocomposites

Ln-POMs and nanocomposites $Na_9[LnW_{10}O_{36}]H_2O@SiO_2$ for the whole Ln series were characterized as previously described for Ln = Eu,Gd,Tb. [46] The hydration number (x) of the $Na_9[LnW_{10}O_{36}].xH_2O$ POMs obtained by elemental analysis, TGA, and FT-IR are collected in Table S1, and the FT-IR data for the corresponding nanocomposites in Table S2. In the nanocomposites, the Ln-POM terminal W=O stretching mode (932-943 cm^{-1}) shifts to higher wavenumbers (943-957 cm^{-1}), while the three Ln-POM W-O-W stretching

modes of the edge-shared WO_6 octahedral moieties (838-896 cm^{-1}, 777-840 cm^{-1} and 704-797 cm^{-1}) are replaced by a single one (788-883 cm^{-1}) in the nanocomposites. [46,50] The latter, exhibit also several SiO_2 vibrations, including the asymmetric stretch mode ν_{as}(Si-O-Si) in the 1080-1050 cm^{-1} region, the symmetric stretch mode ν_s(Si-O-Si) at 798 cm^{-1}, the bending mode δ(Si-O-Si) at 460 cm^{-1} and the stretching mode of the silanol groups at 950 cm^{-1}.

The TEM images of Ln-POMs@SiO_2 show well-defined, morphologically uniform nanospheres, consisting of a POM-containing core coated with an amorphous silica shell (Fig. 2).The average core diameter and shell thickness observed for the NPs studied range from 10 to 28 nm, and 4 to 11 nm, respectively. The average diameter of Eu-POMs@SiO_2 NPs is 35 nm, with a core diameter of 18 nm, giving a silica shell average thickness of 8.5 nm. [46] For most systems, the core size is in a narrow range (18-22 nm), except for La (much smaller, 9.5 nm) and Pr (much larger, 28 nm). However, the NPs total size and silica shell thickness vary considerably: from 23 nm (La) to 43 nm (Pr) for the total size, and from 11 nm (Gd and Tb) to 4 nm (Ho) and 6 nm (Er) for the shell thickness. Our previous studies suggest that the solubility in water of LnPOM influences the NPs core size. [46] The alkaline hydrolysis of TEOS followed by condensation of the silica oligomers, results in the growth of a silica network towards the centre of the reverse micelles, thus entrapping LnPOM in their interior. As a consequence, the core size is also expected to influence the total NPs size, as the same amount of TEOS is used throughout the LnPOM@SiO_2 series. EDX elemental analyses of the nanocomposites was carried out for some of the systems and revealed the presence of Ln, W and Si (Fig. S1). [46] Ln and W (POMs) are present mostly in the NPs cores. [46] Bulk elemental analysis by ICP-MS (Si, Na, W and Ln) of some nanocomposites is given in Table S3, which also shows the calculated molecular formulae, molecular weights and Ln concentrations (mM) in 1 mg/ml aqueous suspensions.

Fig. S2 shows the SEM images of $Na_9[EuW_{10}O_{36}]$@SiO_2 NPs and SiO_2 NPs. In the former, the shape characterization was hampered by the high tendency of the NPs to aggregate.

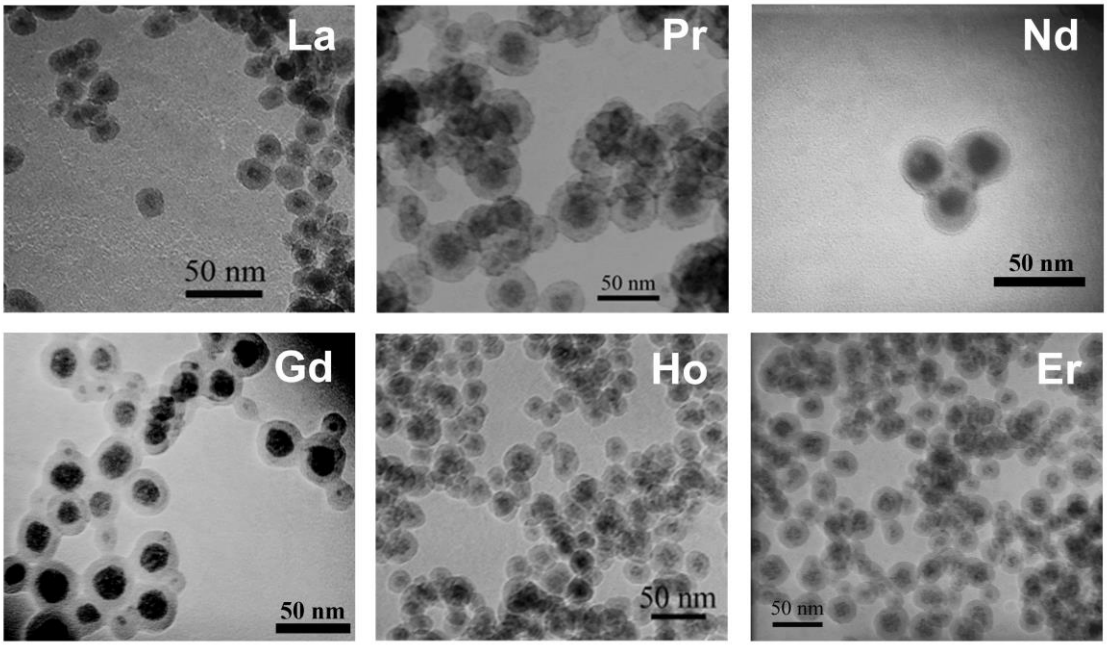

Figure 2. TEM images of $Na_9[LnW_{10}O_{36}]@SiO_2$ (Ln = La^{3+},Pr^{3+}, Nd^{3+}, Gd^{3+}, Ho^{3+} and Er^{3+}) nanocomposites.

The silica layer of the nanocomposites was studied by ^{29}Si solid-state MAS NMR. Figure S3 shows a representative spectrum obtained for a $[Gd(W_5O_{18})_2]@SiO_2$ sample. It contains three resonances at *ca.* −90, −100, and −110 ppm, assigned to Si atoms with two, one and zero attached hydroxyl groups, and two, three and four neighboring $[SiO_4]$ groups, *i.e.*, Q^2, Q^3 and Q^4, respectively. [51] No TEOS signal at -82.0 ppm is observed, indicating that it was consumed in the synthesis. [52] There are also no peaks from surface Si atoms with one neighboring $[SiO_4]$ group and one free or alkylated silanol (Q^1), which should appear in the -81 to -84 ppm range. [52,53] While the Q^4 environment corresponds to bulk Si atoms, the silica layer inner and outer surfaces contain Si atoms with a single attached silanol (Q^3) or two geminal silanols (Q^2). Such silanol groups present at the inner surface of the silica layer could form hydrogen bonds with the negatively charged oxygen atoms of the LnPOM W-O bonds and with water (Figure 1A).

DLS measurements of aqueous suspensions of $Na_9[LnW_{10}O_{36}]H_2O@SiO_2$ nanocomposites (Fig. 3 and Fig. S4) afforded the average hydrodynamic diameters (d_H) and zeta (ζ) potentials listed in Table 1. The average hydrodynamic sizes obtained immediately after sample preparation do not vary much along the Ln series and are only

moderately higher than those determined in the solid state by TEM. The average hydrodynamic size of the Eu/Gd(1:1)-POMs is similar to Eu- and Gd-POMs. However, the average hydrodynamic sizes increase with time after preparation (illustrated for 3 h in Table 1 and Fig. S4), reflecting a time dependent increase of their degree of aggregation. The zeta potentials vary between -32.5 and -40.0 mV, whose negative values result from the negatively charged silanol groups present at the silica shell surface.

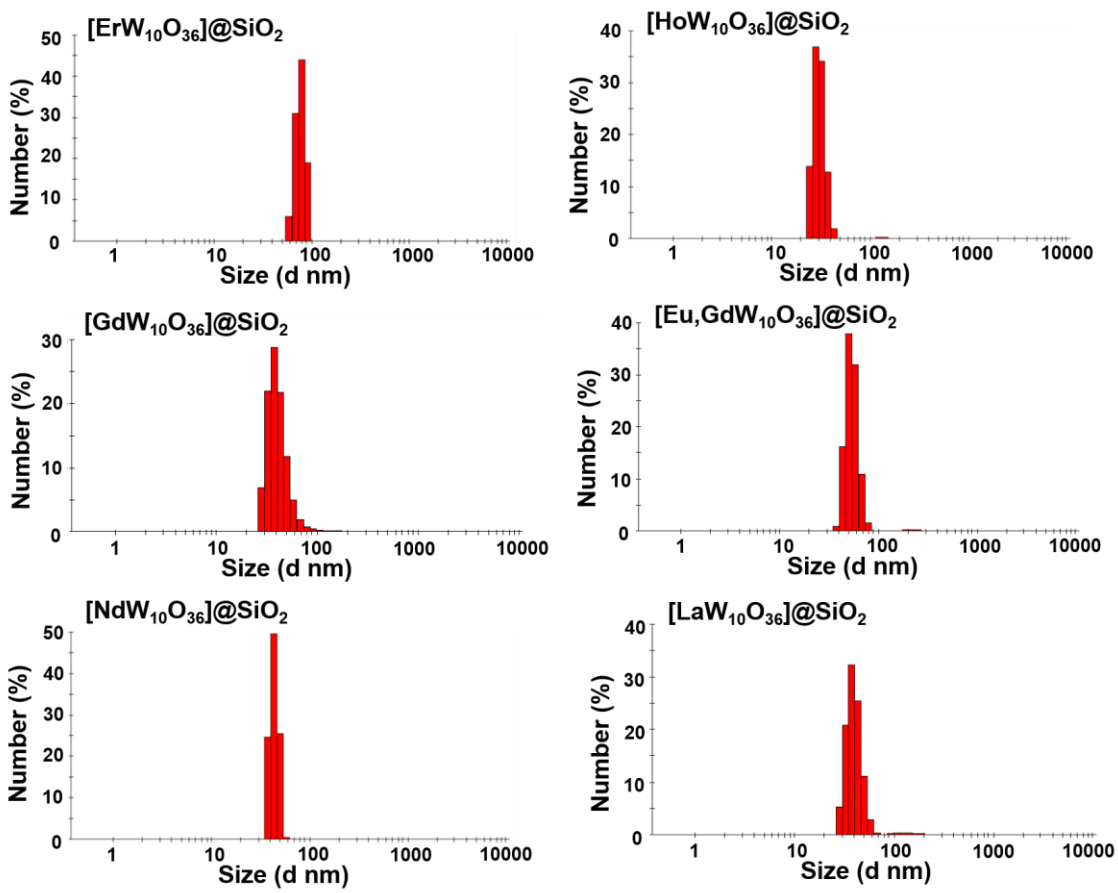

Figure 3. Dynamic Light Scattering measurements of aqueous suspensions of $Na_9[LnW_{10}O_{36}]@SiO_2$ (Ln = La^{3+}, Nd^{3+}, Eu^{3+} + Gd^{3+} (1:1), Gd^{3+}, Ho^{3+} and Er^{3+}) obtained immediately after preparation.

Table 1. Average hydrodynamic diameters (d_H) and zeta (ζ) potentials of aqueous suspensions of $Na_9[LnW_{10}O_{36}]@SiO_2$ nanocomposites obtained by DLS (pH 7.3, 25 °C).

$[Ln(W_5O_{18})_2]@SiO_2$	d_H (nm)	ζ (mv)
La	40.0 ± 9.2	-38.7
Ce	75.2 ± 9.5	-37.0
Pr	57.1 ± 19.9	-34.2
Nd	44.2 ± 4.7	-32.5
Sm	54.5 ± 7.4	-38.8
Eu	50.7 ± 8.2	-38.1
Gd	41.7 ± 12.9	-34.2
Eu/Gd (1:1)	52.7 ± 8.5	[a]
Tb	47.9 ± 6.9	-36.6
Dy	195.1 ± 52.0[b]	-33.3
Ho	30.7 ± 4.4	-36.5
Er	76.6 ± 9.2	-40.0
Tm	115.0 ± 18.0[b]	-34.4
Yb	55.4 ± 12.7	-36.3

[a] Not measured; [b] Measured 3 hours after preparation

Relaxometric studies of LnPOMs and LnPOM@SiO_2 nanocomposites

The r_1 and r_2 relaxivities of GdPOM aqueous solutions at 25 °C and 37 °C were determined at three different magnetic fields/Larmor frequencies, 0.47 T/20 MHz, 9.4 T/400 MHz and 11.7 T/500 Mz (Table 2 and Fig. S5). The r_1 value obtained at 9.4 T and 25 °C is 40 % smaller than r_1 = 6.89 $mM^{-1}{\cdot}s^{-1}$ previously reported in the same conditions using a MRI system instead of an high resolution NMR spectrometer.[39] In all cases, the observed decrease of r_1 and the increase of r_2 with increasing magnetic field, and their decrease with temperature, are in agreement with what is expected from the water proton relaxivities of small Gd^{3+} complexes, which result from the dipolar interaction of the magnetic moment of the Gd^{3+} ion with the magnetic moment of water protons. In principle, they have an inner-sphere (IS) relaxation contribution proportional to the Gd^{3+} water hydration number (q), which involves an efficient exchange of the water

molecules between the inner coordination sphere and the bulk medium, as described by the Solomon-Bloembergen-Morgan (SBM) theory, as well as an outer-sphere (OS) contribution due to the dipolar interaction with the water molecules freely diffusing near the complex.[54] However, the X-ray crystal structure of the LaPOM $Na_2(NH_4)_7[La(W_5O_{18})_2]\cdot 16H_2O$ shows that the central La^{3+} cation links together two $[W_5O_{18}]^{6-}$ anionic fragments binding to eight oxygens in a square antiprismatic coordination geometry, with no inner-sphere water (q = 0) (Fig. 1A). [50] Solid-state luminescence properties of the corresponding EuPOM also show that the Eu^{3+}cation is eight-coordinated with a distorted symmetry very close to D_{4d}, [38] and its dissolution in water does not change the metal's first coordination sphere, as shown by Raman spectroscopy of the isostructural SmPOM polyoxometalate. [55] Thus, it can be assumed that the Gd^{3+} ion in GdPOM also has q = 0 and no IS relaxation contribution. The OS contribution to r_i (i = 1,2) is given by $r_{id}^{OS} \propto (g_J^2 T_{1e}/aD)$, where g_J is the Landé factor of Gd^{3+}, T_{1e} is its electron spin relaxation time, a is the distance of closest approach of a water proton to the Gd^{3+} and D is the relative diffusion constant of OS water molecules. [54] However, the observed relaxivities are too high to be explained solely by the OS contribution, which is expected to be small due to the large value of a resulting from the bulky POM ligands coordinating the Gd^{3+} ion. They can be explained by a large contribution from a 2nd-sphere relaxation mechanism [56,57] comprising the dipolar interaction of Gd^{3+} with a considerable number (q') of water molecules being held for times longer than the translational correlation time (τ_d), in the second coordination shell of Gd^{3+} at a distance r' by hydrogen bonding interactions with the nearby W-O negatively charged oxygen atoms, but that are not directly bound to Gd^{3+} (Fig. 1A). This reasoning is supported by the presence of a large number of water molecules of crystallization involved in an extensive hydrogen bonded network with the $[W_5O_{18}]^{6-}$ anions and the counterions in the crystal structure of the LaPOM. [50] This contribution is represented by $r_{id}^{2S} \propto (\mu_{eff}^2 q'/r'^6)$, where μ_{eff} is the effective magnetic moment of Gd^{3+}.

Table 2. Longitudinal (r_1) and transverse (r_2) water proton relaxivities ($s^{-1}mM^{-1}$) (3% error) of aqueous GdPOM measured at different magnetic fields (B_o)/Larmor frequencies (ω_o) and temperatures.

B_o(T)/ω_o (MHz)	T (°C)	r_1	r_2
0.47/20	25	6.00	6.70
	37	4.32	5.02
9.4/400	25	4.07	7.09
	37	3.10	6.00
11.7 /500	25	4.04	8.53
	37	2.82	7.05

The electron spin relaxation of Gd^{3+} (relaxation time $T_{1e} \cong$ 1-10 ns) is much slower than for the other paramagnetic Ln^{3+} ions ($T_{1e} \cong$ 0.05-2 ps). [58] Therefore, the second sphere and OS contributions to the relaxivities of the non-Gd LnPOM complexes may comprise a dipolar term (r_{id}^{OS}) and a Curie term (r_{iCS}^{OS}). In the fast motion regime, the second sphere terms are represented by $r_{id}^{2S} \propto (\mu_{eff}^2 q' T_{1e}/r'^6)$ and $r_{iCS}^{2S} \propto (\mu_C^2 \tau_R/r'^6)$, where the Curie moment is $\mu_C = \mu_{eff}^2 B_o/3k_B T$, B_o is the magnetic field, T is the absolute temperature, k_B is the Boltzmann constant and τ_R is the rotational correlation time of the complex, while the OS contributions are given by $r_{id}^{OS} \propto (g_J^2 T_{1e}/aD)$ and $r_{iCS}^{OS} \propto (g_J^2 \mu_C^2/aD)$. [28] Therefore, the second-sphere dipolar term is proportional to μ_{eff}^2 and T_{1e}, while the Curie term is proportional to μ_{eff}^4 and B_o^2.

The experimental relaxivities of aqueous solutions of paramagnetic LnPOM (Ln = Eu,Tb-Yb), at 0.47 T and 25 °C, are much lower than those of GdPOM in the same conditions (Table 3). The r_i values of the Ce-Sm complexes are very small (lower than 0.04 $mM^{-1}\cdot s^{-1}$) due to the low μ_{eff} values of these Ln^{3+} ions (not given in Table 2). Assuming that the relaxivities are dominated by the second-sphere mechanism, like for the GdPOM complexes, the small values observed at the low magnetic field (0.47 T) used result from the dominant second-sphere dipolar term, which is small due to the short T_{1e} values and the large value of r'. Their dependence on $\mu_{eff}^2 T_{1e}$ is reflected on their relative values, being largest for Dy and Ho, and smallest for Yb and Eu, in agreement with calculated and experimental values reported for other systems. [58]

Table 3. Longitudinal (r_1) and transverse (r_2) relaxivities ($s^{-1}mM^{-1}$) (3% error) of aqueous LnPOM (Ln= Eu-Yb) measured at 0.47 T and 25 °C.

Ln	r_1	r_2
Eu	0.04	0.05
Gd	6.00	6.70
Tb	0.20	0.25
Dy	0.27	0.36
Ho	0.24	0.32
Er	0.23	0.31
Tm	0.20	0.28
Yb	0.03	0.04

The paramagnetic contributions to the relaxation rates of freshly prepared aqueous suspensions of GdPOM@SiO_2 NPs were obtained at 0.47 T as a function of concentration, at 25 °C and 37 °C (Fig. S6). At 1 mg/mL concentration, the values at 25 °C, R_{1p} = 2.09 s^{-1} and R_{2p} = 2.29 s^{-1}, decrease to R_{1p} = 1.73 s^{-1} and R_{2p} = 1.79 s^{-1} at 37 °C. Considering the percentage of Gd in the NPs ascertained by ICP-MS (Table S3), these rates correspond to relaxivity values r_1 = 10.97 $(mM\ Gd)^{-1}\cdot s^{-1}$ and r_2 = 12.02 $(mM\ Gd)^{-1}\cdot s^{-1}$ at 25 °C, and r_1 = 9.08 $(mM\ Gd)^{-1}\cdot s^{-1}$ and r_2 = 9.40 $(mM\ Gd)^{-1}\cdot s^{-1}$ at 37 °C. These values are about the double of those obtained for the GdPOM solution in the same conditions, in contrast with what is expected from an inefficient OS dipolar relaxation mechanism, due to the increased distance of closest approach of the bulk water molecules to the paramagnetic NPs core due to the 11.0 nm thick silica shell. This is ascribed to the porosity of the silica shell allowing the diffusion of the water molecules to the GdPOM core, as previously observed for core-shell SPION@SiO_2 NPs, whose 8 nm thick silica shell only decreases the r_1 relaxivity by half. [59,60] The relaxivities of Gd-POM@SiO_2 NPs decrease with increasing temperature, indicating that the lifetime of water diffusion inside the silica layer is so short that it does not limit them. The opposite has been found in some mesoporous Gd^{3+}-doped silica-based systems, where a large fraction of Gd^{3+}-complexes immobilized inside their pores, being less accessible to water molecules, are silent from the relaxometric point of view.[19] Similarly, in the Gd^{3+}-doped GdNaY zeolite

the relaxivity increases with the temperature, showing that the proton relaxivity is dominated by slow water exchange, and that the diffusion of water in the zeolite channels to the bulk is its limiting factor.[25] The rotational correlation time (τ_R) of the NPs in water at 25 ^oC , is estimated as 8.40 μs, assuming a spherical shape with an hydrodynamic radius of 21 nm obtained by DLS. This value is too long to limit the observed relaxivities, which can be considered as resulting from a kind of second-sphere effect. They should be a consequence of the paramagnetic effect of Gd^{3+} chelates in the core-shell interface with motion restricted water molecules close to that interface, in fast exchange with bulk water.

At 0.47 T and 25 ^oC, the relaxation rates of the non-Gd LnPOM@SiO_2 suspensions at 1 mg/mL concentration are 1-2 orders of magnitude smaller than for the Gd-NPs, due to the much longer Ln^{3+} T_{1e} values, especially for Ce-Eu and Yb. The contribution of the OS Curie relaxation mechanism is also small at low magnetic fields. The r_i values were not compared along the Ln series because both the NPs core size and silica shell thickness were not constant, with a large impact on their relaxivities.

Replacing half of the Gd^{3+} ions by Eu^{3+} in the Gd:Eu(1:1)-POM@SiO_2 NPs, the relaxivity values obtained in the same conditions are r_1 = 2.16 s^{-1}. (mM^{-1} Gd+Eu) and r_2 = 4.18 s^{-1}. (mM^{-1} Gd+Eu), showing a decrease to 20 % and 35 %, respectively, relative to the values for Gd-POM@SiO_2 s^{-1}. mM^{-1} Gd. This decrease is larger than that (60-62%) observed for 50% replacement of Gd^{3+} by Eu^{3+} in SiO_2@APS-DTPAGd, where the inner-sphere contribution dominates the relaxation by the chelated Ln^{3+} at the particle surface.[20] In the case of the SPION@$Gd(btfa)_3(H_2O)_2$@SiO_2 NPs (btfa = 4,4,4-trifluoro-L-phenyl-1,3-butanedione), a bimodal T_1/T_2 relaxation system with a large contribution to r_2 from the SPION and a smaller r_1 contribution from the Gd^{3+} complex embedded in the porous silica shell, the 50% replacement of Gd^{3+} by Eu^{3+} leads to a 70% increase of r_1 and a 63% decrease of r_2 at 9.4 T.[30]

The relaxation behavior of the suspensions could not be studied at 11.7 T due to their instability at high magnetic fields. Therefore, the dependence of R_2 on the τ_{CP} values in a CPMG sequence, which informs on the T_2 relaxation regime present for the NPs, could not be studied. The previously studied Ln_2O_3 nanoparticles [61] and Ln-AV9 zeolite nanoparticles [32] showed very large and τ_{CP}-dependent r_2 values, characteristic of the static dephasing relaxation regime (SDR), where the condition $\tau_D >> 1/\Delta\omega$ occurs,

where τ_D is the diffusion correlation time of the NPs and $\Delta\omega$ is the difference in Larmor frequency at the particle surface and that at infinity. In this case, the water proton diffusion is slower than the spatial variation of the local field inhomogeneities produced by each particle. [28,31,32,61] For other systems, r_2 values are independent of τ_{CP}, and the motional narrowing regime occurs, where the relaxivity is governed by the water diffusion [62-64] in the outer-sphere relaxation mechanism. [65] This should be situation for the NPs studied in this work ($\tau_D << 1/\Delta\omega$), as $\Delta\omega$ should be quite small due to the large silica shell thickness and the small enough size of the particles ($\tau_D < 1x10^{-6}$ s).

Conclusion

Highly increased per-Gd relaxivities have been obtained through the non-covalent confinement of Gd^{3+} complexes in water-permeable nanosystems, such as silica (microporous or mesoporous),[18-22] hydrophilic organic colloids and hydrogels, [23,66,67] apoferritin, [68] zeolites,[24,25] as well as carbon nanotubes,[26] fullerenes[27] and nanocomposites incorporating these into mesoporous silica nanodiscs.[69] In this study, the relaxivities of the core-shell NPs, prepared by encapsulating $[Ln(W_5O_{18})_2]^{9-}$ polyoxometalates (LnPOM) within amorphous silica shells ($Ln(W_5O_{18})_2]@SiO_2$) were studied along the Ln series.

$K_9[Gd(W_5O_{18})_2]$ POM has been previously assessed as MRI contrast agent *in vitro* and *in vivo*.[39] The present study found a decrease of r_1 and increase of r_2 with increasing magnetic field, as expected for small Gd^{3+} chelates. These relaxivities are slightly higher than those of typical clinically used MRI CAs, such as Gd-DTPA (Magnevist®). In $[Gd(W_5O_{18})_2]^{9-}$, the Gd^{3+}ion has no inner-sphere water ($q = 0$) in the coordination sphere, as witnessed by X-ray crystallography of the corresponding LaPOM, [50] solid-state luminescence data of EuPOM, [38] and Raman spectroscopy of SmPOM. [55] Thus, in the absence of inner-sphere relaxation, the GdPOM relaxivity is attributed to second-sphere relaxation. At a low magnetic field (0.47 T), the non-Gd paramagnetic LnPOMs exhibit small r_i values ($r_1 < r_2$), due to the small second-sphere dipolar relaxation resulting from the combined effects of the short T_{1e} values of the Ln^{3+} ions and the large distance between the water molecules and Ln^{3+} brought about by the bulky POM anions. Their relative values depend on $\mu_{eff}^2 T_{1e}$, being largest for Dy and Ho, and smallest for Yb and Eu. [60]

$[Ln(W_5O_{18})_2]@SiO_2$ NPs were characterized along the lanthanide series in the solid state and in aqueous suspensions. In the solid state, they have a core-shell spherical structure, with a LnPOM-core coated with amorphous silica, whose core diameter and shell thickness are not uniform along the Ln series, ranging from 28/8 nm for Pr to 22/10 nm for Tb. In aqueous suspensions, the NPs zeta potentials range between -32.5 and -40.0 mV, and hydrodynamic sizes are time dependent, being in the 31-77 nm range for freshly prepared suspensions, which are only moderately larger than in the solid state. However, these values increase with time, up to 195 nm at 3 h, reflecting the formation of larger aggregates, despite the favorable zeta potentials.

The 0.47 T and 25 ^oC relaxivities of $GdPOM@SiO_2$ NPs aqueous suspensions r_1 = 10.97 $(mM\ Gd)^{-1}\cdot s^{-1}$ and r_2 = 12.02 $(mM\ Gd)^{-1}\cdot s^{-1}$ are considerably larger than for GdPOM solutions in the same conditions. This is so even if the presence of a 11.0 nm thick silica shell is expected to keep the outer-sphere water molecules far from the GdPOM core, making the OS dipolar relaxation mechanism very inefficient. Those values can be explained by the considerable porosity of the amorphous silica shell, as observed before in core-shell $SPION@SiO_2$ nanoparticles[59,60] This second-sphere effect was magnified by the long rotational correlation time of the NPs, but the concentration of the GdPOM complexes in the core surrounded by the silica shell limited their water access to those at the core surface. This arrangement contributed to the much smaller relaxivity values than those obtained for spherical $[Gd(ebpatcn)(H_2O)]@SiO_2$ NPs (ebpatcn = 1-carbo xyethyl-4,7-bis((6-carboxypyridin-2-yl)methyl)-1,4,7-triazacyclononane) with wider silica pore channels and a random distribution of the Gd^{3+} complexes in the silica matrix through electrostatic and hydrogen-bonding interactions.[21] This distribution allowed the complexes to not mutually hinder the accessibility of the water molecules to the Gd^{3+} ions, while their mobility and that of water molecules were restricted by confinement in the silica matrix. These structural and dynamic properties led to high r_1 and r_2 values, with both inner and outer-sphere contributions. [21]

In the same experimental conditions, the relaxation effects of non-Gd $LnPOM@SiO_2$ NPs suspensions are 1-2 orders of magnitude smaller than Gd-NPs due to the much longer Ln^{3+} T_{1e} values, especially for Ce-Eu and Yb. However, their comparison along the Ln series was hampered by the different core size and silica shell thickness, which strongly affect the relaxivities. The NPs form unstable water suspensions at high

magnetic field (11.7 T). Their stabilization using, e.g., xanthan gum, and synthesis of core-shell structures of identical sizes along the Ln series, will enable a more thorough characterization of their relaxation properties. This work is in progress.

Co-doping of the Gd-POM@SiO_2 NPs by replacement of half of the Gd^{3+} ions by Eu^{3+}, leading to Gd:Eu(1:1)-POM@SiO_2 NPs, decreases their r_1 and r_2 relaxivities at 0.47 T to 20 % and 35 % of their initial values, which are still substantial. The comparison of the steady-state spectra and quantum yields of Gd:Eu(1:1)-POM@SiO_2 NPs and Eu-POM@SiO_2 NPs showed no effective interaction between Gd^{3+} and Eu^{3+} ions, like in other Gd/Eu co-doped systems,[20] with an unchanged quantum yield of 0.08.[46] In conclusion, the fair relaxivities and the suitable photoluminescence properties observed for the Gd:Eu(1:1)-POM@SiO_2 NPs indicate that they have potential to be used as dual modality CAs for MRI and optical imaging.

Experimental Section

All reagents were purchased from Aldrich and used without further purification. The lanthanopolyoxometalates, $Na_9[Ln(W_5O_{18})_2]\cdot xH_2O$ (Ln = La, Ce, Pr, Nd, Sm, Eu, Gd, Tb, Dy, Ho, Er, Tm, Yb), were prepared using the method described by Peacock and Weakley. [70] The corresponding $Na_9[LnW_{10}O_{36}]$@SiO_2 nanocomposites were prepared by a reverse microemulsion method (W/O, water in oil microemulsions) for the hydrolysis of tetraethoxysilane (TEOS), [71] as previously described. [46] Nanocomposites containing 1:1 mole ratio of the Eu^{3+} and Gd^{3+} and Eu^{3+} and Tb^{3+} complexes were also prepared. Fourier Transform infrared spectra (FT-IR) were recorded on a Mattson 7000 spectrophotometer using KBr pellets. Spectra in the ATR acquisition mode used a Specac MKII Golden Gate attenuated reflectance system. Thermogravimetric analysis (TGA) was carried out on a Shimadzu – TGA 50 Thermogravimetric Analyser, with a heating rate of 10.0 ^oC/min up to 800 ^oC. The morphology of the samples was studied on a Hitachi H-9000 microscope in the scanning electron microscopy (SEM) and transmission electron microscopy (TEM) modes, operated at 300 kV. High-resolution TEM (HRTEM) and elemental mapping by X-ray energy dispersive spectroscopy (EDX) analysis were carried out on a JEOL 2200FS transmission electron microscope operating at an acceleration voltage of 200 kV. Drops of diluted dispersions of NPs were air-dried on carbon films deposited on 200-mesh copper grids. The excess liquid was blotted with filter paper.

Dynamic Light Scattering (DLS) measurements of aqueous suspensions of the NPs (without surfactant) were carried out on a Malvern ZetaSizer Nano ZS series model Zen3500 equipment (Malvern, UK). The hydrodynamic size and zeta potential of the NPs dispersed in water by ultrasonication were obtained using the ZS Xplorer software (Malvern Panalytical). ^{29}Si solid-state NMR spectra were recorded at 79.50 MHz on a Bruker Avance III 400 (9.4 T) wide-bore spectrometer. Samples were packed into 7 mm diameter zirconia rotors and spun at the magic-angle at 5 kHz. ^{29}Si chemical shifts are quoted in ppm from TMS. ^{1}H NMR relaxation experiments were carried out on a Bruker Minispec relaxometer (0.47 T/20 MHz), and Bruker Avance III 400 (9.4 T/400.13 MHz) and Bruker Avance IIIHD 400 (11.7 T/500.13 MHz) NMR spectrometers. Water proton longitudinal relaxation times (T_1) were measured using the inversion recovery pulse sequence, while the water proton transverse relaxation times (T_2) were measured using a Carr-Purcell-Meiboon-Gill (CPMG) pulse sequence. The reported values are the averages over three different measurements. All experimental relaxation rates ($R_i = 1/T_i$) were corrected for diamagnetic contributions using aqueous suspensions of the La^{3+}-containing NPs in the same conditions. The Ln concentrations were determined by Inductively Coupled Plasma Mass Spectrometry (ICP-MS).

Acknowledgements

This work was developed within the scope of the project CICECO-Aveiro Institute of Materials, UIDB/50011/2020 & UIDP/50011/2020, financed by national funds through the Portuguese Foundation for Science and Technology (FCT)/MCTES. CFGCG thanks the FCT for funding the Coimbra Chemistry Centre through the programmes UIDB/00313/2020 and UIDP/00313/2020, also co-funded by FEDER/COMPETE 2020-EU.

Keywords: Contrast agents; Core-shell nanoparticles; Lanthanide complexes; Paramagnetic relaxation; Polyoxometalates

References

[1] R. Weissleder, U. Mahmood, *Radiology*, **2001**, *219*, 316–333.

[2] P. Caravan, Z. Zhang in *The Chemistry of Contrast Agents in Medical Magnetic Resonance Imaging* (Eds.: A. E. Merbach, L. Helm, É. Tóth) 2nd ed., John Wiley & Sons Ltd, Chichester, **2013**, pp. 311–342.

[3] E. Gianolio, R. Stefania, E. Di Gregorio, S. Aime, *Eur. J. Inorg. Chem.,* **2012**, 1934–1944.

[4] J. Wahsner, E. M. Gale, A. Rodríguez-Rodríguez, P. Caravan, *Chem. Rev*., **2019,** *119*, 957−1057.

[5] M. A. McDonald, K. L. Watkin, *Acad. Radiol*., **2006**, *13*, 421–427.

[6] J. B. Livramento, A. Sour, A. Borel, A. E. Merbach, É. Tóth, *Chem. Eur. J.*, **2006**, *12*, 989–1003.

[7] R. N. Muller, A. Roch, J.-M. Colet, A. Ouakssim, P. Gillis in *The Chemistry of Contrast Agents in Medical Magnetic Resonance Imaging* (Eds.: A. E. Merbach, L. Helm, É. Tóth) 1st ed., John Wiley & Sons Ltd, Chichester, **2001**, pp. 417-435.

[8] Q. A. Pankhurst, J. Connolly, S. K. Jones, J. Dobson, *J. Phys. D: Appl. Phys.,* **2003**, *36*, R167–R181.

[9] J.-L. Bridot, A.-C. Faure, S. Laurent, C. Rivière, C. Billotey, B. Hiba, M. Janier, V. Josserand, J.-L. Coll, L. Vander Elst, R. N. Muller, S. Roux, P. Perriat, O. Tillement, *J. Am. Chem. Soc*., **2007**, *129*, 5076–5084.

[10] W. Zhang, J. Martinelli, F. Mayer, C. S. Bonnet, F. Szeremeta, K. Djanashvili, *RSC Adv*., **2015**, *5*, 69861-69869.

[11] H. Hifumi, S. Yamaoka, A. Tanimoto, D. Citterio, K. Suzuki, *J. Am. Chem. Soc.*, **2006**, *128*, 15090-15091.

[12] C. Frangville, M. Gallois, Y. Li, H. H. Nguyen, N. Lauth-de Viguerie, D. R Talham, C. Mingotaud, J.-D. Marty, *Nanoscale*, **2016**, *8*, 4252–4259.

[13] P. J. Debouttière, S. Roux, F. Vocanson, C. Billotey, O. Beuf, A. Favre-Réguillon, Y. Lin, S. Pellet-Rostaing, R. Lamartine, P. Perriat, O. Tillement, *Adv. Funct. Mater.*, **2006**, *16*, 2330-2339.

[14] M. F. Ferreira, B. Mousavi, P. M. Ferreira, C. I. O. Martins, L. Helm, J. A. Martins, C. F. G. C. Geraldes, *Dalton Trans.*, **2012**, *41*,5472-5475.

[15] M. F. Ferreira, J. Goncalves, B. Mousavi, M. I.M. Prata, S. P. J. Rodrigues, D. Calle, P. Lopez-Larrubia, S. Cerdan, T. B. Rodrigues, P. M. Ferreira, L. Helm, J. A. Martins, C. F. G. C. Geraldes, *Dalton Trans*., **2015,** *44*, 4016-4031.

[16] M. I. A. Pereira, G. Pereira, C. F. G. C. Geraldes, P. E. Cabral Filho, C. L. Cesar, A. A. de Thomaz, B. S. Santos, G. A. L. Pereira, A. Fontes, *Sci. Reports*, **2019**, *9*, 2341.

[17] D. Ho, X. Sun, S. Sun, *Acc. Chem. Res*., **2011**, *44*, 875-882.

[18] J. A. Peters, K. Djanashvili, *Eur. J. Inorg. Chem*., **2012**, 1961-1974.

[19] F. Carniato, L. Tei, M. Botta, *Eur. J. Inorg. Chem*. **2018**, 4936–4954.

[20] S. L. C. Pinho, H. Faneca, C. F. G. C. Geraldes, M.-H. Delville, L. D. Carlos, J. Rocha, *Biomaterials*, **2012**, *33*, 925-935.

[21] N. Wartenberg, P. Fries, O. Raccurt, A. Guillermo, D. Imbert, M. Mazzanti, *Chem. Eur. J.* **2013**, *19*, 6980 – 6983.

[22] S. Fedorenko, A. Stepanov, R. Zairov, O. Kaman, R. Amirov, I. Nizameev, K. Kholin, I. Ismaev, A. Voloshina, A. Sapunova, M. Kadirov, A. Mustafina, *Colloids and Surfaces A* **2018**, *559*, 60–67.

[23] R. Zairov, S. Pizzanelli, A. P. Dovzhenko, I. Nizameev, A. Orekhov, N. Arkharova, S. N. Podyachev, S. Sudakova, A. R. Mustafina, L. Calucci, *J. Phys. Chem. C* **2020**, *124*, 4320−4329.

[24] S. W. Young, F. Qing, D. Rubin, K. J. Balkus, Jr., J. S. Engel, J. Lang, W. C. Dow, J. D. Mutch, R. A. J. Miller, *Magn. Reson. Imaging*, **1995**, *5*, 499–508.

[25] C. Platas-Iglesias, L. Vander Elst, W. Zhou, R. N. Muller, C. F. G. C. Geraldes, T. Maschmeyer, J. A. Peters, *Chem. Eur. J*., **2002**, 8, 5121-5131.

[26] H. Gong, R. Peng, Z. Liu, *Adv. Drug Delivery Rev*. **2013**, *65*, 1951–1963.

[27] K. B. Ghiassi, M. M. Olmstead, A. L. Balch, *Dalton Trans*., **2014**, *43*, 7346-7358.

[28] M. Norek, J. A. Peters, *Progr. Nucl. Magn. Reson. Spectr*., **2011**, *59*, 64-82.

[29] G. Goglio, G. Kaur, S. L. C. Pinho, N. Penin, A. Blandino, C. F. G. C. Geraldes, A. Garcia, M.-H. Delville, *Eur. J. Inorg. Chem*., **2015**, 1243-1253.

[30] S. L. C. Pinho, J. Sereno, A. J. Abrunhosa, M.-H. Delville, J. Rocha, L. D. Carlos, C. F. G. C. Geraldes, *Inorg. Chem.* **2019**, *58*, 16618−16628.

[31] G. A. Pereira, M. Norek, J. A. Peters, D. Ananias, J. Rocha, C. F. G. C. Geraldes, *Dalton Trans.* **2008**, 2241–2247.

[32] G. A. Pereira, J. A. Peters, F. A. Almeida Paz, J. Rocha, C. F. G. C. Geraldes, *Inorg. Chem*., **2010**, *49*, 2969-2974 2969.

[33] J. Iball, J. N. Low, T. J. R. Weakley, *J. Chem. Soc. Dalton Trans*. **1974**, 2021–2024.

[34] T. Yamase, T. Ozeki, *Acta Crystallogr., Sect. C: Struct. Chem*., **1993**, *49*, 1577-1580.

[35] T. Yamase, T. Ozeki, M. Tosaka, *Acta Crystallogr., Sect. C: Struct. Chem*., **1994**, *50*, 1849-1852.

[36] J.-C. G. Bünzli, *Acc. Chem. Res*., **2006**, *39*, 53-61.

[37] T. Yamase in *Handbook on the Physics and Chemistry of Rare Earths* (Eds: J.-C. G. Bünzli, K. A. Gschneidner, K. P. Vitalij), Elsevier, **2009**, Vol. 39, Chapter 243, pp- 297-356.

[38] R. A. Sá Ferreira, S. S. Nobre, C. M. Granadeiro, H. I. S. Nogueira, L. D. Carlos, O. L. Malta, *J. Lumin.*, **2006**, *121*, 561-567.

[39] J. Feng, X. Li, F. Pei, G. Sun, X. Zhang, M. Liu, *Magn. Reson. Imaging*, **2002**, *20*, 407-412.

[40] J. Feng, G. Sun, F. Pei, M. Liu, *J. Inorg. Biochem.*, **2002**, *92*, 193-199.

[41] Z. Li, W. Li, X. Li, F. Pei, Y. Li, H. Lei, *Magn. Reson. Imaging*, **2007**, 27, 412-417.

[42] W. J. Crooks III, G. R. Choppin, B. E. Rogers, M. J. Welch, *Nucl. Med. Biol*., **1997**, *24*, 123-125.

[43] C. E. VanPelt, W. J. Crooks III, G. R. Choppin, *Inorg. Chim. Acta*, **2002**, *340*, 1-7.

[44] E. Kanal, M. F. Tweedle, *Radiology*, **2015**, *275*, 630-634.

[45] E. Brücher, G. Tircsó, Z. Baranyai, Z. Kovács, A.D. Sherry in *The Chemistry of Contrast Agents in Medical Magnetic Resonance Imaging* (Eds.: A. E. Merbach, L. Helm, É. Tóth) 2nd ed., John Wiley & Sons Ltd, Chichester, **2013**, pp. 157-208.

[46] C. M. Granadeiro, R. A. Sá Ferreira, P. C. R. Soares-Santos, L. D. Carlos, T. Trindade, H. I. S. Nogueira, *J. Mat. Chem*., **2010**, *20*, 3313-3318.

[47] L. Frullano, T. J. Meade, *J. Biol. Inorg. Chem*., **2007**, *12*, 939-949.

[48] K. Yan, P. Li, H. Zhu, Y. Zhou, J. Ding, J. Shen, Z. Li, Z. Xu, P. K. Chu, *RSC Adv*., **2013**, *3*, 10598-10618.

[49] H. F. Wehrl, S. Wiehr, M. R. Divine, F. C. Maier, A.-M. Rolle, B. J. Pichler, S. Gatidis, G. T. Gullberg, J. Schwenck, W. M. Thaiss, *J. Nucl. Med*. **2014**, 11S-18S.

[50] F. A. Almeida Paz, M. S. S. Balula, A. M. V. Cavaleiro, J. Klinowski, H. I. S. Nogueira, *Acta Cryst*., **2005**, *E61*, i28-i31.

[51] G. E. Maciel, D. W. Sindorf, *J. Am. Chem. Soc.*, **1980**, *102*, 7606−7607.

[52] F. Devreux, J. P. Boilot, F. Chaput, *Phys. Rev. A*, **1990**, *41*,6901-6909.

[53] A. Tuel, H. Hommel, A. P. Legrand, E. S. Kovats, *Langmuir*, **1990**, *6*, 770–775.

[54] É. Tóth, L. Helm, A. E. Merbach in *The Chemistry of Contrast Agents in Medical Magnetic Resonance Imaging* (Eds.: A. E. Merbach, L. Helm, É. Tóth) 2nd ed., John Wiley & Sons Ltd, Chichester, **2013,** pp. 25–81.

[55] W. P. Griffith, R. G. H. Moreea, H. I. S. Nogueira, *Polyhedron*, **1996**, *15*, 3493-3500.

[56] M. Botta, *Eur. J. Inorg. Chem.* **2000**, 399-407.

[57] G. A. Pereira, J. A. Peters, E. Terreno, D. Delli Castelli, S. Aime, S. Laurent, L. Vander Elst, R. N. Muller, C. F. G. C. Geraldes, *Eur. J. Inorg. Chem*., **2012**, 2087-2098.

[58] I. Bertini, C. Luchinat, G. Parigi, E. Ravera, *NMR of Paramagnetic Molecules: Applications to Metallobiomolecules and Models,* 2nd Edition, Elsevier, Amsterdam, **2017**

[59] S. L. C. Pinho, G. A. Pereira, P. Voisin, J. Kassem, V. Bouchaud, L. Etienne, J. A. Peters, L. D. Carlos, S. Mornet, C. F. G. C. Geraldes, J. Rocha, M.-H. Delville, *ACS Nano*, **2010**, *4*, 5339–5349.

[60] S. L. C. Pinho, S. Laurent, J. Rocha, A. Roch, M.-H. Delville, L. D. Carlos, L. Vander Elst, R. N. Muller, C.F.G.C. Geraldes, *J. Phys. Chem. C*, **2012**, *116*, 2285-2291.

[61] M. Norek, G. A. Pereira, C. F. G. C. Geraldes, A. Denkova, W. Zhou, J. A. Peters, *J. Phys. Chem. C*, **2007**, *111*,10240-10246

[62] P. Gillis, F. Moiny, R. A. Brooks, *Magn. Reson. Med.*, **2002**, *47*, 257–263.

[63] R. N. Muller, P. Gillis, F. Moiny, A. Roch, *Magn. Reson. Med*. **1991**, *22*, 178–182.

[64] M. Norek, E. Kampert, U. Zeitler, J. A. Peters, *J. Am. Chem. Soc.*, **2008**, *130*, 5335-5340.

[65] R. A. Brooks, F. Moiny, P. Gillis, *Magn. Reson. Med.*, **2001**, *45*, 1014–1020.

[66] T. Courant, V. G. Roullin, C. Cadiou, M. Callewaert, M. C. Andry, C. Portefaix, C. Hoeffel, M. C. Goltstein, M. Port, S. Laurent, L. V. Elst, R. N. Muller, M. Molinari, F. Chuburu, *Angew. Chem. Int. Ed.* **2012**, *51*, 9119 – 9122.

[67] S. Figueiredo, J. N. Moreira, C. F. G. C. Geraldes, S. Rizzitelli, S. Aime, E. Terreno, *Chem. Commun*., **2011**, *47*, 10635–10637.

[68] S. Aime, L. Frullano, S. G. Crich, *Angew. Chem. Int. Ed.* **2002**, *41*, 1017 – 1019.

[69] J. S. Ananta, B. Godin, R. Sethi, L. Moriggi, X. W. Liu, R. E. Serda, R. Krishnamurthy, R. Muthupillai, R. D. Bolskar, L. Helm, M. Ferrari, L. J. Wilson, P. Decuzzi, *Nat. Nanotechnol.* **2010**, *5*, 815 –821.

[70] R. D. Peacock, T. J. R. Weakley, *J. Chem. Soc. A*, **1971**, 1836 – 1839.

[71] Z. Ye, M. Tan, G. Wang, J. Yuan, *J. Mater. Chem*., **2004**, *14*, 851- 856.